BNL-216032-2020-JAAM

Growth and structural studies of In/Au(111) alloys and InOx/Au(111) inverse oxide/metal model catalysts

J. Kang, J. A. Rodriquez

To be published in "Journal of Chemical Physics"

February 2020

Chemistry Department

Brookhaven National Laboratory

U.S. Department of Energy

USDOE Office of Science (SC), Basic Energy Sciences (BES) (SC-22)

Notice: This manuscript has been authored by employees of Brookhaven Science Associates, LLC under Contract No. DE-SC0012704 with the U.S. Department of Energy. The publisher by accepting the manuscript for publication acknowledges that the United States Government retains a non-exclusive, paid-up, irrevocable, world-wide license to publish or reproduce the published form of this manuscript, or allow others to do so, for United States Government purposes.

DISCLAIMER

This report was prepared as an account of work sponsored by an agency of the United States Government. Neither the United States Government nor any agency thereof, nor any of their employees, nor any of their contractors, subcontractors, or their employees, makes any warranty, express or implied, or assumes any legal liability or responsibility for the accuracy, completeness, or any third party's use or the results of such use of any information, apparatus, product, or process disclosed, or represents that its use would not infringe privately owned rights. Reference herein to any specific commercial product, process, or service by trade name, trademark, manufacturer, or otherwise, does not necessarily constitute or imply its endorsement, recommendation, or favoring by the United States Government or any agency thereof or its contractors or subcontractors. The views and opinions of authors expressed herein do not necessarily state or reflect those of the United States Government or any agency thereof.

Growth and Structural Studies of In/Au(111) Alloys and InO_x/Au(111) Inverse Oxide/Metal Model Catalysts

Jindong Kang, [a] Mausumi Mahapatra,[b] Ning Rui,[b] Ivan Orozco,[a] Rui Shi,[a] Sanjaya D. Senanayake,[b] and José A. Rodriguez [a,b] *

[a] Department of Chemistry, SUNY at Stony Brook, Stony Brook, NY, 11794 USA

[b] Chemistry Department, Brookhaven National Laboratory, Upton, NY, 11973 USA

* Corresponding author, E-mail: rodriguez@bnl.gov

Abstract

Indium oxide has received attention as an exciting candidate for catalyzing the CO_2 hydrogenation to methanol due to its high selectivity (>80%). Compared to the extent of research on the activity of indium oxide-based powder catalysts, very little is known about the phenomena associated with the formation of surface alloys involving indium or the growth mechanism for indium oxide nanoparticles. In this report, scanning tunneling microscopy (STM) and X-ray photoelectron spectroscopy (XPS) were employed to elucidate the growth mode, structure, and chemical state of In/Au(111) alloys and InO_x/Au(111) inverse model catalysts. Our study reveals distinct morphological differences between In/Au(111) and InO_x/Au(111), and the InO_x structure also depends strongly on the preparation conditions. In/Au surface alloy systems with extremely low coverage (0.02 ML) form islands preferentially on the elbow sites of reconstructed Au(111) herringbone, regardless of hcp and fcc stacking. At higher coverage (0.1 ML), the In islands expand over the herringbone in the <110> direction and create two dimensional domain structures over the entire surfaces. Moreover, this 2D domain structure is disturbed by temperature with high dispersion of indium atoms observed during the annealing process. Oxidation of the In/Au(111) surface alloys with O_2 at 550 K produces InO_x/Au(111) systems which contain various sizes of InO_x aggregates (from 0.7 to 10 nm). On the other hand, InO_x/Au(111) surfaces prepared by vapor deposition of In at 550 K in an O_2 background exhibit highly dispersed and uniformly small InO_x particles (~1 nm). Both InO_x systems were confirmed to be partially oxidized by XPS.

Introduction

Methanol synthesis from CO_2 hydrogenation ($CO_2 + 3H_2 \rightarrow CH_3OH + H_2O$) is an attractive way to produce valuable chemicals by exploiting anthropogenic CO_2, a major greenhouse gas, mitigating its level in the air. Particularly, since methanol has advantages of being used as feedstock for production of value-added chemicals and as an alternative energy fuel, many research efforts have been made in heterogenous catalysis considering such economic and environmental merits of CO_2 hydrogenation to methanol.[1–6] The commercial catalyst for methanol synthesis involves a mixture of $Cu/ZnO/Al_2O_3$, and methanol is produced from syngas ($CO_2/CO/H_2$) over this Cu-based catalyst at elevated temperature (493−573 K) and pressures (5−10 MPa).[7,8] However, for the direct hydrogenation of CO_2, this catalyst has explicit limitations due to its limited activity, low stability, and low selectivity toward methanol, since CO_2 hydrogenation to methanol has to compete with the concurring reverse water-gas shift reaction (RWGS: $CO_2 + H_2 \rightarrow CO + H_2O$), and the by-product water inhibits the activity, subsequently leading to sintering of the active phase under reaction condition.[9]

For these reasons, novel catalysts with different configurations have been proposed and reported. Indium oxide has recently drawn a great deal of attention as an exciting candidate for CO_2 hydrogenation to methanol[4–6,10–13]. Recent studies on indium oxide based catalysts have shown their high catalytic selectivity for methanol synthesis.[10,11] Especially, due to the suppression of the RWGS, a high CO_2 selectivity on indium oxide based catalysts is reported in methanol steam reforming, which is the reverse reaction of CO_2 hydrogenation to methanol.[14] Density-functional theory (DFT) calculations have identified oxygen vacancies as potential active sites for indium oxide catalysts, which can help CO_2 activation and hydrogenation by stabilizing the key intermediates involved in methanol formation.[12,13] Therefore, the unique properties of indium oxide-based catalysts make them an attractive

candidate for methanol synthesis, warranting that further studies will be performed with these systems.

Recent studies on catalytic activity and DFT-based electronic properties have shown high performance and potential active sites, but the distinct experimental identification of these active sites in terms of structure and morphology remain elusive. To design and optimize these metal oxide-based catalysts, it is necessary to obtain a deeper understanding of the nature of active sites by structural characterization and to discover the structure – property relationship from these studies. In heterogeneous catalysts, inverse oxide/metal catalysts have been extensively adopted as model systems to gain mechanistic and structural insight in industrial catalysts.[15–18] For example, nanoparticles of titania, ceria and iron oxide has been deposited on a Au(111) substrate producing systems with structural and electronic properties not seen in the bulk oxides.[15,18] In principle, oxide nanoparticles exhibit novel electronic properties resulting from their size and high density of defects relative to their bulk oxide counterpart.[19] Inverse model catalysts often exhibit higher catalytic activity than that of conventional metal/oxide-based catalysts because reactants can interact with the defect sites of the oxide nanoparticles as well as metal sites and the metal–oxide interface on the surface.[1,20,21] Like in the case of indium oxide, it has been reported that defect sites such as oxygen vacancies in metal oxides promote CO_2 adsorption and activation in methanol synthesis.[12] In this regard, placing the oxide phase on top of metal substrate can increase the probability for CO_2 adsorption on the surface, facilitating subsequent reaction steps in the methanol synthesis process.

Recent studies using high-resolution transmission electron microscopy (HRTEM) and DRIFT spectroscopy have identified the formation of a ZnO overlayer on Cu particles during the CO/CO_2 hydrogenation reaction in conventional $Cu/ZnO/Al_2O_3$ catalysts for methanol synthesis.[22,23] This finding suggests that an inverse catalyst configuration is a likely active

phase of commercial catalysts. These perspectives serve as motivation for an investigation of the inverse model InO_x/Au(111) catalysts in this paper along with In/Au(111) surface alloys as a comparison. Although bulk gold is known to be catalytically inactive, gold surfaces covered by small oxide nanoparticles show activities better than or comparable to those of benchmark catalysts.[21,20] In the case of TiO_x/Au(111) and CeO_x/Au(111), these catalysts facilitate the WGS reaction (WGS: $CO + H_2O \rightarrow CO_2 + H_2$) by providing active sites for water dissociation on oxygen vacancies within the oxide nanoparticles and CO adsorption on Au sites, with subsequent reactions occurring at metal-oxide interface sites.[21]

In the first section of this article, we use scanning tunneling microscopy (STM) to characterize the structure of In/Au (111) surface alloys prepared by vapor depositing indium metal onto a gold substrate at 300 K and the resulting morphological changes after annealing to temperature as high as 650 K. We also discuss the early nucleation stage from a lower coverage and illustrate the evolution of the indium adlayer up to a coverage of about 0.1 monolayer (ML). This would make this work relevant to those interested in metal-on-metal growth and metal/metal interfaces, which serve as the foundation for bimetallic heterogeneous catalysts. Next, the structure and chemical state of inverse InO_x/Au catalysts are investigated by STM and X-ray photoelectron spectroscopy (XPS). Two different types of InO_x/Au morphologies were prepared following two different preparation methods, and their structural variations will be discussed in the second part of the article.

2. Experimental Methods

All the STM experiments were conducted using an Omicron STM instrument housed in an ultra-high vacuum chamber with a background pressure of 5×10^{-10} Torr. A Au(111)

single crystal (MaTeck) was cleaned by cycles of Ar ion sputtering and annealing (850 K for 10 min and 650K for 30min).[24] The STM images were collected at 300 K by using a Pt–Ir tip. Indium was vapor-deposited at 300K on the clean Au(111) substrate by using a commercial metal evaporator (Omicron) to form In/Au alloys, and Indium oxide was prepared by oxidizing the In/Au(111) alloys at 600 K with 5 x 10^{-7} Torr of O_2 or by vapor depositing indium at 600 K directly under an atmosphere of oxygen (5 x 10^{-7} torr). The preparation methods for our InO_x films on the Au single crystal surface were adopted and modified from those of our previously reported study for ZnO films, which provided the inverse ZnO/Cu configuration seen in HRTEM images for the conventional catalysts for methanol synthesis.[3,25] To estimate coverage and particle size for the InO_x nanoparticles, we considered sets of images and the average sizes of more than 50 clusters. Different bias voltage was applied during the measurements, but high-resolution images, which are clear enough to detect InO_x clusters or measure their sizes, were only obtained within the certain voltage range reported below in the paper. Within that range, the height did not change. A code was used to calculate the In or InOx coverage by calculating the area of protrude features on the surface.

Ambient pressure XPS (AP-XPS) experiments were performed using an instrument available at the Chemistry Department of Brookhaven National Laboratory (BNL). A commercial SPECS AP-XPS chamber equipped with a PHOIBOS 150 EP MCD-9 analyzer and a Mg Kα anode was used to record the Au 4f, In 3d, O 1s, and In MNN regions. A Au(111) single crystal, cleaned by cycles of Ar ion sputtering and annealing (850 K, 10 min and 650K for 30min), was used as a substrate to grow In or InO_x overlayers. Nanoparticles of InO_x were deposited following the same methodology applied to the STM experiments described above. InO_x clusters were obtained by vapor-depositing indium at 600 K directly under an atmosphere of oxygen (P_{O2} ~ 5 x 10^{-7} Torr). The formation of InO_x over the gold substrate was verified by

means of Auger electron spectroscopy (AES). The surface coverage for the XPS data was calculated by the peak attenuation of Au after depositing In or InO_x on a clean Au(111) whose baseline was obtained first.

3. Results and Discussion

3.1 Preparation of In/Au(111) surface alloys

Indium and gold can form different types of binary alloys (Au_4In, Au_3In, Au_7In3, AuIn, $AuIn_2$, etc).[26] The two metals exhibit a large miscibility even at room temperature. These alloys are stable up to temperatures above 800 K.[26,27] In the past, Auger electron spectroscopy, electron-energy-loss spectroscopy, low-energy electron diffraction (LEED) and work-function change measurements have been used to investigate the growth of indium on a Au(111) substrate.[27] It was found that an alloy, $AuIn_2$, was formed from the onset of deposition and the alloy thickened a layer at a time.[27] Alloy formation modified the electronic properties of the bonded metals.[27] This was the starting point for our STM studies.

Figure 1a presents a typical reconstructed Au(111) surface with the characteristic herringbone structure.[28,29] This well-known Au(111) (22 x $\sqrt{3}$) reconstruction structure is created by a unidirectional contraction of the topmost gold layer along the <110> directions, in which two extra gold atoms are packed into the surface layer every 22 lattice spacings in the <110> direction. This leads to a lattice mismatch between the surface and bulk atomic spacings and appear as bright pairs of lines, called soliton walls, ridges, or discommensuration lines, in STM images.[30] The soliton walls distinguish two alternating regions of hexagonally closed packed (hcp) and face centered cubic (fcc) domain, and when two soliton walls meet, they produce edge dislocations at the elbows with under-coordinated surface atoms so that it makes

the elbows the most reactive areas of the Au(111) surface.[29–31]

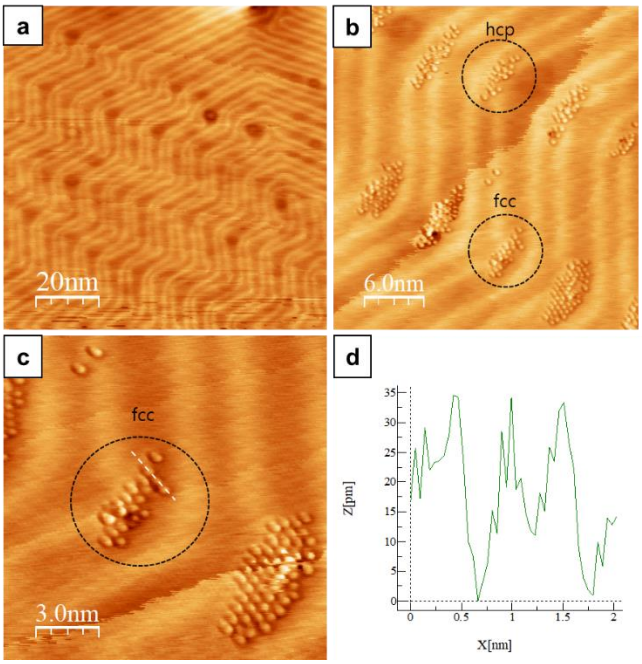

Figure 1. STM images of 0.025 ML In/Au(111) collected at 300K: (a) reconstructed clean Au(111) surface (100 x 100 nm^2), (b) Indium islands formed at herringbone elbow sites (30 x 30 nm^2), (c) close-up image (15 x 15 nm^2), (d) a line profile measurement of an indium island in Figure 1c. Images were collected at 0.08 nA, -1 V for (a) and 0.1 nA, -1.3 V for (b,c) as tunneling conditions.

After a low coverage of indium (0.025 ML) was vapor-deposited onto Au(111) at 300K, indium metal formed islands at the elbows of the gold herringbone structure (Figure 1b). Specifically, it is observed that indium islands tend to locate in the narrowed regions within the elbows. Similar behavior has been also observed for the growth of Ni and Cu on Au (111).[30, 31] Wang *et al*. found Ni island formation at elbows and proposed that adatoms initially exchange with Au atoms at edge dislocations of the Au herringbone reconstruction. Those surface-layer atoms then become nucleation sites for subsequent atoms to form islands.[31] Similarly, Figure 1 provides evidence that at room temperature, indium incorporation into gold takes place by gold atom displacement at areas close to the discommensuration line of the (22×√3) reconstruction, with islands then developing in the adjacent narrowed region, irrespective of fcc and hcp

stacking. The line profile in Figure 1d presents that each circular feature indicates atomic indium (~0.5 nm in size) and it is embedded into the gold surface. Hence the height of indium atoms is measured only about ~0.35 Å. An exchange of In and Au atoms to form a surface alloy is consistent with the large miscibility of these two metals.[26] It agrees with previous results of LEED for the In/Au(111) system.[27]

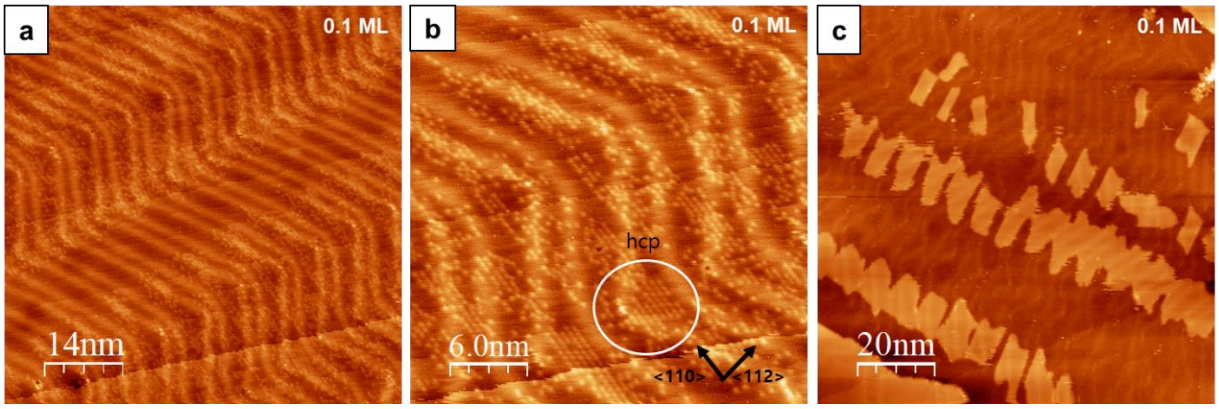

Figure 2. STM images of 0.1 ML In/Au(111) collected at 300 K: (a) 70 x 70 nm^2, (b) 30 x 30 nm^2, (c) 100 x 100 nm^2. Imaging conditions: 0.09 nA, -1.4 V (a,b) and 0.07 nA, 1 V (c).

To better understand the growth behavior of indium on gold, we increased the coverage of indium from 0.025 ML to 0.1 ML (Figure 2). With an increase in the In dose, the indium metal grows from the elbows of the gold herringbone and expands from there sideways in the <110> direction, creating domains with ordered structure. Upon this observation, we can conclude that the indium deposited on the gold substrate follows a Frank–van der Merwe mode of growth, in which adatoms form a two-dimensional layer on the substrate, pointing to a strong interaction between gold and indium which leads to alloy formation. A similar growth behavior was reported by Chang *et al.*; when indium was deposited on Au (50 nm thick) coated NaCl, a $AuIn_2$ phase was spontaneously formed at the interface (a phenomenon, confirmed by X-ray diffraction).[32] According to Robison *et al.*, a surface alloy with a $AuIn_2$ phase develops from the onset of In deposition on the Au(111) substrate at room temperature.[27] Our observation is

also in line with the idea of minimizing the surface free energy: Since gold has a higher surface free energy (1.185 J m^{-2}) than indium (0.556 J m^{-2}),[32] the indium should disperse on the surface laterally and wet instead of forming three-dimensional (3D) clusters or diffusing into the bulk of the gold sample. Different from Figure 2a and 2b, Figure 2c is obtained by altering the tip condition and indium deposits appear as a film or patch shapes on the gold surface. At this higher coverage, broader hcp areas (white circle, Figure 2b) are more occupied with indium although the admetal is also present in narrowed regions on both fcc and hcp symmetry.

To understand the effect of temperature on the behavior of indium on the gold surface, we annealed the sample from 300 to 650 K and probed into its surface with STM upon cooling back to room temperature. Figure 3 shows the corresponding surface of the annealed In/Au alloys, where the increase in temperature caused the indium atoms to disperse randomly over the surface. The previously observed well-ordered structure of indium deposits at room temperature lost its periodicity and indium atoms were found at both hcp and fcc regions after 450 K. The herringbone ridges is raised about 0.2 Å with respect to the surrounding areas,[29] and at low coverage, indium was first deposited on hollow sites and then expanded to ridges as the coverages increase. However, after high temperature annealing, indium is almost equally found at ridge sites compared to the hollow sites. Furthermore, given the binding energies of In-Au (286.0 kJ/mol) and of In-In (82.0 kJ/mol),[33] the In-Au interaction is much stronger than the In-In interaction, and such strong bonding is maintained even at elevated temperature. Hence, indium demonstrates a preference to spread out over the entire gold substrate.

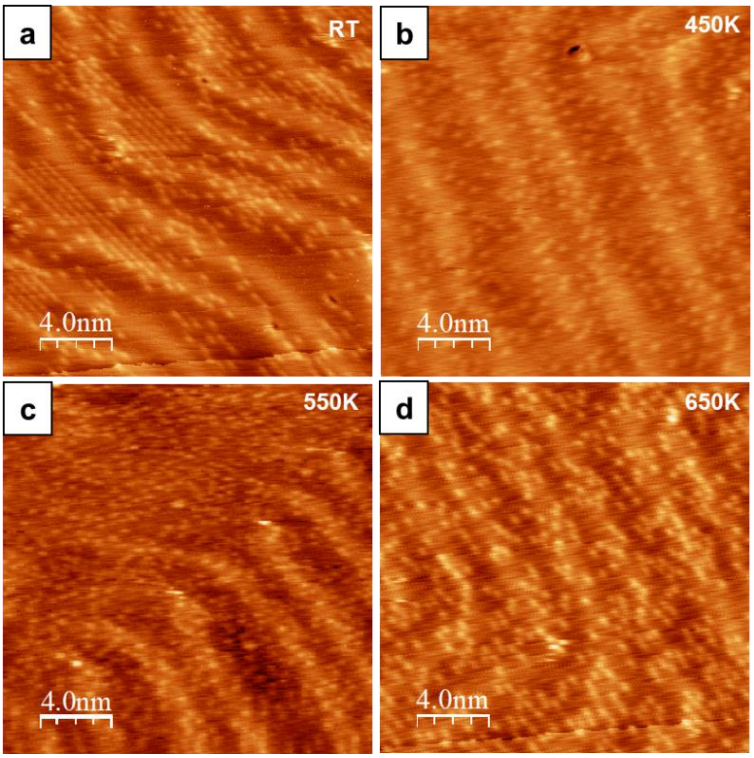

Figure 3. STM images of 0.1ML In/Au(111) obtained (a) at room temperature, and after annealing : (b) 450 K (c) 550 K, (d) 650 K. Images were collected at 300 K, 20 x 20 $nm^{2.}$ (0.07 ~ 0.1 nA, -1.4 ~ 0.9 V).

3.2 Oxidation of In/Au alloy surfaces at 550K

Following our previous studies for the formation of the inverse ZnO/Cu catalyst,[3,25] we examined different approaches for the formation of InO_x on Au(111). In one of them, 0.025 or 0.1 ML of In were vapor-deposited onto Au(111) at 300 K followed by oxidation with 5×10^{-7} Torr of O_2 for 20 min at 550 K. Figures 4 and 5 show as-prepared InO_x/Au(111) catalysts with 0.025 and 0.1 ML of indium, respectively. The formation of InO_x aggregates on various sizes is noticeable after high temperature oxidation, which was not observed in the previous In/Au alloys systems even at elevated temperatures. At 0.025 ML, the size of the oxide particles falls in the range between 0.7 and 10 nm with 0.5 Å – 4 nm in height. The line profile measurements in Figure 4 were done over the particles in Figure 4b and represent the average

sizes of InO_x as prepared. An increase in indium coverage to 0.1 ML did not lead to a big difference in morphology but increased the number of large InO_x nanoparticles: Large particles are more frequent in Figure 5a than in Figure 4a. From this observation, it can be said that oxygen links to the indium on/in the surface and builds up oxide particles, overcoming the In-Au interfacial interaction. This idea is consistent with the fact that the In-O bond (346kJ/mol) is substantially stronger than the In-Au bond (286kJ/mol).[33] Therefore, the formation of oxide particles by oxidation of In/Au(111) systems can be explained by the perspective of a larger binding energy. The chemical state of this oxide was examined by XPS/AES and a typical Auger spectrum is displayed in Figure 5b. According to the literature,[34] the kinetic energies of bulk In_2O_3 and In metal within the In MNN region appear at 410.4 eV and 406.4 eV, respectively, whereas our prepared InO_x shows a peak at 408.7 eV. Therefore, our model catalysts are partially oxidized when compared to In_2O_3. Additionally, Dai *et al*. has found a rapid phase transformation from In to an intermediate InO_y at an oxygen exposure of 1000 Langmuir on an In foil.[35] This result is in a good agreement with our result where an intermediate indium oxide (In^{1+} or In^{2+}) has been formed by reaction of O_2 with In/Au(111).

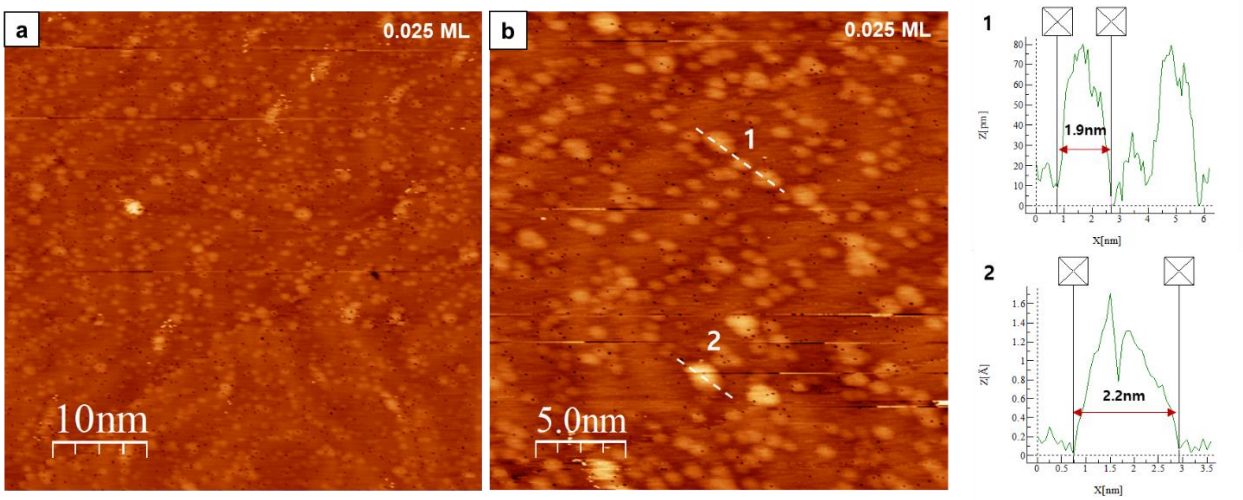

Figure 4. STM images of 0.025 ML InO_x/Au(111) prepared by oxidation of In/Au(111) at 550K: (a) 50 x 50 nm^2 and (b) 25 x 25 nm^2. Images were collected at 300 K (0.07 nA, -1.2 V). The line profile measurements were carried out over the numbered particles (1, 2) in the STM

images.

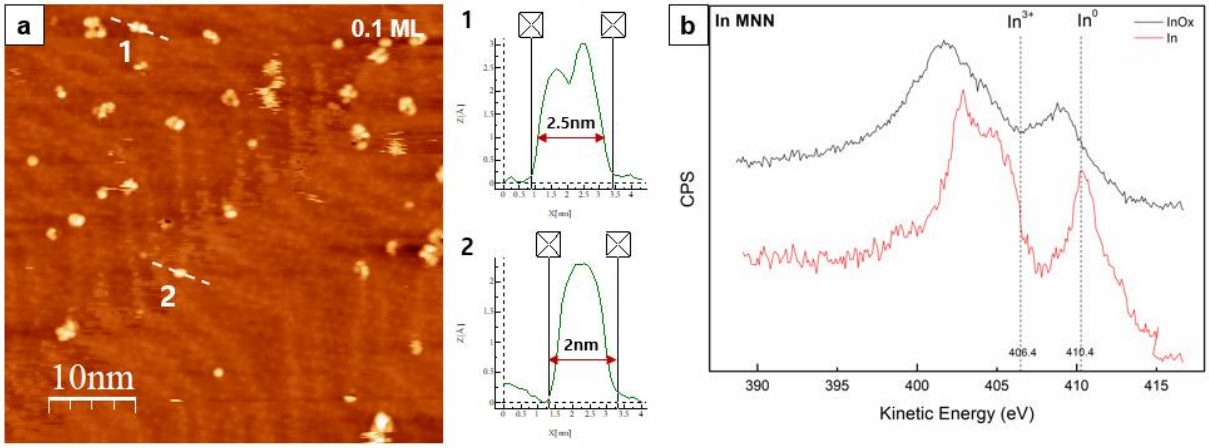

Figure 5. STM images of 0.1 ML InO_x/Au(111) prepared by oxidation of In/Au(111) at 550 K : (a) 50 x 50 nm^2. Images were collected at 300 K (0.09 nA, -1 V). The line profile measurements were carried out over the numbered particles (1 - 2) in the STM images. (b) Indium MNN AES spectra collected after depositing In on Au(111) and then subsequently oxidizing at 550 K.

3.3 In deposition on Au(111) in an oxygen environment at 550K

It has been reported that direct deposition of an element under an O_2 environment can lead to the formation of novel oxide nanostructures giving inverse oxide/metal catalysts unique physical and chemical properties.[3,25,36] In a second type of synthetic approach, reactive deposition was employed, and InO_x/Au(111) systems were produced by vapor depositing indium metal onto the gold substrate under an O_2 background ($5x10^{-7}$ Torr) at 550 K. Figure 6a and 6b displays 0.025 ML and 0.1 ML of InO_x prepared by reactive deposition, respectively. The morphology of these oxides is quite different from that of InO_x made by oxidation of the In-Au alloy systems at 550 K (Figures 4 and 5). This type of InO_x consists of a uniform array of small clusters, and big particle formation was rarely observed. The insets in Figure 6a and 6b represents the line profile measurements across the as prepared InO_x clusters. According to the measurements, for 0.025 ML, the size and height of InO_x clusters range from 0.6 to 1 nm and 0.35 – 0.7 Å, respectively. For 0.1 ML, they are determined to be 0.7 - 1nm in size and 0.2 – 0.4 Å in height. The size of these clusters is comparable to the lattice parameter of In_2O_3 in a

cubic unit cell, which is 1.0115 nm.[37] This seems to be a characteristic of nonstoichiometric In_2O_{3-x} due to the presence of oxygen vacancies. A decrease in the unit cell parameter of In_2O_{3-x} was also observed in Au-In_2O_3 nanocomposites after annealing.[38] The chemical state of the InO_x/Au(111) system was studied by photoemission, and the AES spectrum in Figure 6c determines that the indium overlayer is partially oxidized (In^{1+} or In^{2+}), displaying a peak at 409.3 eV.

In the images shown in Figures 5a and 6b, one obtained by the oxidation of a In/Au surface alloy and the other by direct reactive deposition, the surface morphology is very different although the total coverage of indium is the same. This phenomenon can be attributed to a variation in the oxygen chemical potential. It has been shown that the oxygen chemical potential during growth affects surface diffusion altering the nature of adsorbed species and leading to significant variations in morphology.[39] This phenomenon can be applied to our model systems since, under the oxygen-rich environment of Figure 6, a In-O bond may be formed without previously breaking a In-Au bond. In the O_2/In/Au(111) systems shown in Figures 4 and 5, there is a balance between the cleavage of In-Au bonds and the formation of In-O bonds, which conditions the mobility of In and the reaction to form InO_x particles. In the alloys, the indium atoms are at specific sites of the gold surface and only on these locations the particles of InO_x can grow. Thus, by tuning the initial state and the growth conditions, the two approaches examined in this study lead to different surface morphologies for InO_x/Au opening the possibility for important variations in the catalytic properties of this metal-oxide interface. It is interesting to notice that in the case of InO_x/Au(111), one obtains oxide nanoparticles much smaller than those seen after depositing titania, ceria and iron oxide on a Au(111) substrate.[15,18] This probably reflects very strong oxide-metal interactions in the InO_x/Au(111) system which probably lead to special catalytic properties unique for this interface.[10,11]

Recent studies on indium oxide based powder catalysts have shown their high catalytic selectivity for methanol synthesis.[10,11] In principle, using the model systems shown in Figures 4-6, one can investigate how the size and shape of indium oxide nanoparticles affect the binding of CO_2, the dissociation of H_2, and the hydrogenation of HCO_x fragments. In the case of TiO_x/Au(111) and CeO_x/Au(111), previous studies have shown that the addition of very small amounts of the oxide adlayer (0.05-0.15 ML) to the gold substrate substantially enhances the catalytic properties of the system producing excellent catalysts for CO_2 hydrogenation, the water-gas shift reaction, and CO oxidation.[15,17,20,21,40] In the case of CO_2 hydrogenation, the small nanoparticles of the oxide form an interface with gold that is very efficient for binding and transforming CO_2 into CO and methanol.[40] Unfortunately, neither titania nor ceria can give the high selectivity for a $CO_2 \rightarrow CH_3OH$ transformation seen on indium oxide based catalysts.[10,11] The InO_x/Au(111) systems prepared in this study can be used to study how indium oxide interacts with CO_2 and hydrogen to facilitate an effective $CO_2 \rightarrow CH_3OH$ conversion.

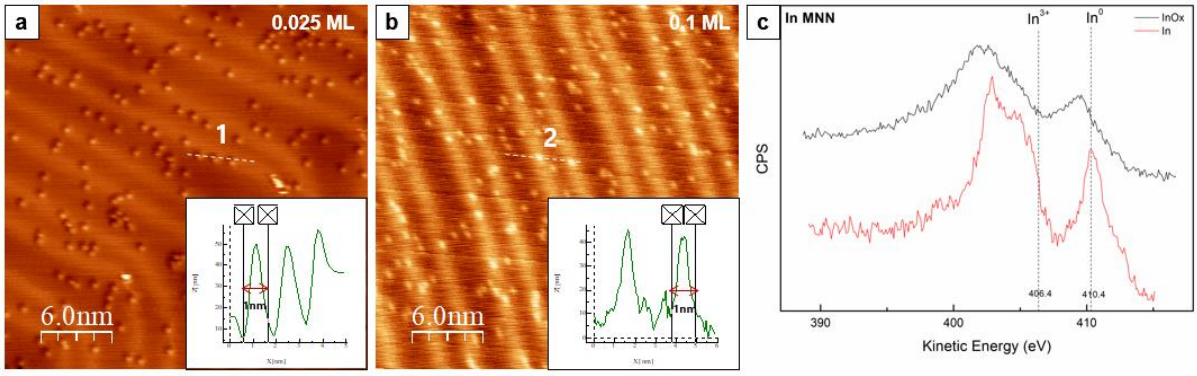

Figure 6. STM images of InO_x/Au(111) prepared by vapor depositing In on Au(111) in oxygen ambient at 550K: (a) 0.025ML, 30 x 30 nm^2 and (b) 0.1ML, 30 x 30 nm^2. Images were collected at 300K (0.1 nA, -1 V). In MNN AES spectra collected after depositing In on Au(111) in O_2 ambient at 550K.

Conclusions

The growth mode and structure of small coverages of In metal and InO_x ($\theta \leq 0.1$ monolayer) on a Au(111) substrate were studied using STM and XPS. For an In/Au(111) surface alloy with an admetal coverage of 0.02 ML, indium islands formed preferentially at the elbow regions of the gold herringbone reconstruction. As the indium coverage increased, the admetal grew two dimensionally, wetting the surface. Thus, the overlayer followed a Frank–van der Merwe mode of growth, implying that the interaction between In adatoms and the Au substrate was stronger than the In-In interaction. Annealing did not promote In-In bonding but provided the adatoms with a higher degree of freedom dispersing them on the gold substrate. For the InO_x/Au(111) systems, two different preparation methods were employed to generate InO_x islands on gold. The oxidation of In-Au alloys produced InO_x nanoparticles ranging from 0.7 to 10 nm on the Au(111) substrate. In contrast, the reactive deposition of In under an O_2 environment at 500–600 K produced highly dispersed clusters of InO_x having sizes smaller than or equal to 1nm. Both deposition methods produced InO_x which was identified as partially oxidized (In^{1+} or In^{2+}) by XPS characterization.

Acknowledgement

The research carried out at Brookhaven National Laboratory was supported by the U.S. Department of Energy, Office of Science and Office of Basic Energy Sciences under contract No. DE-SC0012704. SDS is supported by a U.S. DOE Early Career Award. PR is grateful for financial support by BID and EN-SCN.

References

[1] R.M. Palomino, P.J. Ramírez, Z. Liu, R. Hamlyn, I. Waluyo, M. Mahapatra, I. Orozco, A. Hunt, J.P. Simonovis, S.D. Senanayake, and J.A. Rodriguez, J. Phys. Chem. B **122**, 794 (2018).

[2] A. García-Trenco, A. Regoutz, E.R. White, D.J. Payne, M.S.P. Shaffer, and C.K. Williams, Appl. Catal. B Environ. **220**, 9 (2018).

[3] M. Mahapatra, J. Kang, P.J. Ramírez, R. Hamlyn, N. Rui, Z. Liu, I. Orozco, S.D. Senanayake, and J.J. Rodriguez, J. Phys. Chem. C **122**, 53 (2018).

[4] N. Rui, Z. Wang, K. Sun, J. Ye, Q. Ge, and C.-J. Liu, Appl. Catal. B Environ. **218**, 488 (2017).

[5] J. Ye, C.J. Liu, D. Mei, and Q. Ge, J. Catal. **317**, 44 (2014).

[6] A. Tsoukalou, P.M. Abdala, D. Stoian, X. Huang, M.-G. Willinger, A. Fedorov, and C.R. Müller, J. Am. Chem. Soc. **141**, 13497 (2019).

[7] K.C. Waugh, Catal. Today **15**, 51 (1992).

[8] M. Behrens, F. Studt, I. Kasatkin, S. Kühl, M. Hävecker, F. Abild-Pedersen, S. Zander, F. Girgsdies, P. Kurr, B.-L. Kniep, M. Tovar, R.W. Fischer, J.K. Nørskov, and R. Schlögl, Science **366**, 893 (2012).

[9] M.B. Fichtl, D. Schlereth, N. Jacobsen, I. Kasatkin, J. Schumann, M. Behrens, R. Schlögl, and O. Hinrichsen, Appl. Catal. A Gen. **502**, 262 (2015).

[10] O. Martin, A.J. Martín, C. Mondelli, S. Mitchell, T.F. Segawa, R. Hauert, C. Drouilly, D. Curulla-Ferré, and J. Pérez-Ramírez, Angew. Chemie - Int. Ed. **55**, 6261 (2016).

[11] K. Sun, Z. Fan, J. Ye, J. Yan, Q. Ge, Y. Li, W. He, W. Yang, and C.J. Liu, J. CO2 Util. **12**, 1 (2015).

[12] J. Ye, C. Liu, D. Mei, and Q. Ge, ACS Catal. **3**, 1296 (2013).

[13] M.S. Frei, M. Capdevila-Cortada, R. García-Muelas, C. Mondelli, N. López, J.A. Stewart, D. Curulla Ferré, and J. Pérez-Ramírez, J. Catal. **361**, 313 (2018).

[14] H. Lorenz, W. Jochum, B. Klötzer, M. Stöger-Pollach, S. Schwarz, K. Pfaller, and S. Penner, Appl. Catal. A Gen. **347**, 34 (2008).

[15] J.A. Rodríguez and J. Hrbek, Surf. Sci. **604**, 241 (2010).

[16] C Rameshan, H Li, K Anic, M Roiaz, V Pramhaas, R Rameshan, R Blume, M Hävecker, J Knudsen, A Knop-Gericke, G Rupprechter, J. Phys.: Condens. Matter **30**, 264007 (2018)

[17] J.A. Rodriguez, J. Graciani, J. Evans, J.B. Park, F. Yang, D. Stacchiola, S.D. Senanayake, S. Ma, M. Perez, P. Liu, J.F. Sanz, and J. Hrbek, Angew. Chemie - Int. Ed. **48**, 8047 (2009).

[18] J. Zhang and J.W. Medlin, Surf. Sci. Rep. **73**, 117 (2018).

[19] M. Fernández-García, A Martínez-Arias, J.C. Hanson, J.A. Rodriguez, Chem. Rev. **104**, 4063 (2004).

[20] R.M. Palomino, R.A. Gutiérrez, Z. Liu, S. Tenney, D.C. Grinter, E. Crumlin, I. Waluyo, P.J. Ramírez, J.A. Rodriguez, and S.D. Senanayake, ACS Sustain. Chem. Eng. **5**, 10783 (2017).

[21] J.A. Rodriguez, S. Ma, P. Liu, J. Hrbek, J. Evans, and M. Pérez, Science **318**, 1757 (2007).

[22] T. Lunkenbein, J. Schumann, M. Behrens, R. Schlögl, and M.G. Willinger, Angew. Chemie - Int. Ed. **54**, 4544 (2015).

[23] J. Schumann, J. Kröhnert, E. Frei, R. Schlögl, and A. Trunschke, Top. Catal. **60**, 1735 (2017).

[24] S.D. Senanayake, D. Stacchiola, P. Liu, C.B. Mullins, J. Hrbek, and J.A. Rodriguez, J. Phys. Chem. C **113**, 19536 (2009).

[25] M. Mahapatra, R.A. Gutiérrez, J. Kang, N. Rui, R. Hamlyn, Z. Liu, I. Orozco, P.J. Ramírez, S.D. Senanayake, and J.A. Rodriguez, Surf. Sci. **681**, 116 (2019).

[26] M. Hansen, *Constitution of Binary Alloys* (McGrow-Hill, New York, 1958).

[27] M. Robinson and A. Slavin, Phys. Rev. B - Condens. Matter Mater. Phys. **54**, 14087 (1996).

[28] C. Woll, S. Chiang, R.J. Wilson, and P.H. Lippel, Phys. Rev. B **39**, 7988 (1989).

[29] J. V Barth, H. Brune, G. Ertl, and R.J. Behm, Phys. Rev. B **42**, 15 (1990).

[30] F. Grillo, H. Früchtl, S.M. Francis, and N. V. Richardson, New J. Phys. **13**, (2011).

[31] Z.T. Wang, M.T. Darby, A.J. Therrien, M. El-Soda, A. Michaelides, M. Stamatakis, and E.C.H. Sykes, J. Phys. Chem. C **120**, 13574 (2016).

[32] Z.C. Chang, F.H. Lu, and F.S. Shieu, Mater. Chem. Phys. **70**, 137 (2001).

[33] Y. Luo, *CRC Handbook of Chemistry and Physics*, 90th ed., edited by D. R. Lide (CRC Press/Taylor and Francis, Boca Raton, 2009).

[34] D. Wagner, M. Riggs, E. Davis, F. Moulder, E. Muilenberg, *Handbook of X-Ray Photoelectron Spectroscopy* (Perkin-Elmer Corporation, Physical Electronics Division, Eden Prairie, Minn., 1979).

[35] D. Dai, F. Zhu, Appl. Surf. Sci. **59**, 195 (1992).

[36] L. Yu, Y. Liu, F. Yang, J. Evans, J. A. Rodriguez, P. Liu, J. Phys. Chem. C **119**, 16614 (2015).

[37] D.R. Hagleitner, M. Menhart, P. Jacobson, S. Blomberg, K. Schulte, E. Lundgren, M. Kubicek, J. Fleig, F. Kubel, C. Puls, A. Limbeck, H. Hutter, L.A. Boatner, M. Schmid, and U. Diebold, Phys. Rev. B **85**, 115441 (2012).

[38] M.I. Ivanovskaya, E.A. Ovodok, and D.A. Kotsikau, Glas. Phys. Chem. **37**, 560 (2011).

[39] G. Franceschi, M. Wagner, J. Hofinger, T. Krajňák, M. Schmid, U. Diebold, and M. Riva, Phys. Rev. Mater. **3**, (2019).

[40] J. Graciani, K. Mudiyanselage, F. Xu, A.E. Baber, J. Evans, S.D. Senanayake, D.J. Stacchiola, P. Liu, J. Hrbek, J.F. Sanz, and J.A. Rodriguez, Science, **345**, 546 (2014).